Optics Letters

Resonance-free ultraviolet metaoptics via photon nanosieves

Juan Li,[1,†] Guangyuan Si,[2,†] Hong Liu,[3] Jiao Lin,[2] Jinghua Teng,[3] and Kun Huang[1,*]

[1]Department of Optics and Optical Engineering, University of Science and Technology of China, Anhui 230026, China
[2]School of Engineering, RMIT University, Melbourne, Victoria 3001, Australia
[3]Institute of Materials Research and Engineering, Agency for Science, Technology and Research, 2 Fusionopolis Way, Innovis, #08-03, Singapore 138634, Singapore
*Corresponding author: huangk17@ustc.edu.cn

Received 16 April 2019; revised 30 May 2019; accepted 3 June 2019; posted 13 June 2019 (Doc. ID 365010); published 3 July 2019

Ultraviolet (UV) light with high-energy photons is widely used in various areas such as nano-lithography, biology, and photoemission spectroscopy. The flexible control over its amplitude and phase is a longstanding problem due to the strong absorption from most materials. Here, we propose a nano-aperture platform to control the amplitude and phase of UV light and experimentally demonstrate amplitude- and phase-type holograms at a wavelength of 355 nm. In principle, nano-apertures etched on a metal film can be filled in vacuum, so that the material issue about optical absorption is not involved in this configuration, allowing us to manipulate UV light through the geometry of nano-apertures even when plasmonic resonances are absent. A binary-amplitude nanosieve is used to reconstruct three holographic images at different cut-planes by tuning the constructive interference elaborately. Meanwhile, rectangular nano-apertures are employed to demonstrate UV holograms with geometric phase that is controlled by the orientation of the nano-apertures. This platform could be extended to other UV regions. © 2019 Optical Society of America

https://doi.org/10.1364/OL.44.003418

Ultraviolet (UV) light plays an important role in many applications because it can provide high-energy photons for changing the chemical and physical properties of illuminated objects [1], or exciting the photoemission of materials in angle-resolved photoemission microscopy [2], or manipulating the radiation of quantum emitters [3]. Due to the limited bandgap, most materials have strong absorption in the UV spectrum [4], which makes it challenging to manipulate UV light. Compared with the visible and infrared optics, the UV components are less developed, so that only lenses, gratings, dielectric mirrors, condensers, and zone plates are available in the UV spectrum. These UV elements are made of either bulky volume or transparent rings, or periodic structures that have a limited degree of freedom. Therefore, developing micro-/nano-devices with arbitrary or customized arrangements will enrich the family of UV optics.

Recently, ultrathin metasurfaces [5–7] made of spatially varied subwavelength structures have caught tremendous attention due to their superior ability to manipulate amplitude, phase, and polarization of light through electromagnetic interaction. In comparison with traditional optical devices, metasurfaces have advantages such as miniaturized volume, polarization sensitivity, high-resolution pixels, and multiplexing of multiple functionalities [8], which are attractive in developing UV optics. Based on the fundamental mechanism of metasurfaces, two approaches can be used to design meta-structures in the UV region. One is to shape the electromagnetic responses by using well-designed nano-structures made of transparent and high-refractive-index materials [4] or metals [9] supporting plasmonic resonances. For example, dielectrics such as Nb_2O_5 [4], ZnO [10], and Si [11] have been demonstrated as materials of UV metasurfaces with efficiency as high as ~80% [4]. The metallic meta-structures made of Al [12] and Rh [13] are also used to excite UV plasmonics for applications of metasurfaces. This approach depends highly on materials that have optical properties of low absorption and high refractive indices, which is available only at UV wavelengths from ~130 – 400 nm. For UV light with even smaller wavelengths such as extreme UV (EUV) and soft x rays where all materials are absorbing [1], metasurfaces can be made by utilizing the nano-apertures etched in an opaque thin film, which is considered as the second approach of UV metasurfaces. No material is filled in the nano-aperture, so that it significantly releases the dependence of materials, which therefore makes it feasible in the entire electromagnetic spectrum. Such a nano-aperture approach has been reported as amplitude-modulated metasurfaces in the visible and infrared regions [14–19], where optical plasmonics can be excited easily to enhance efficiency. However, no plasmonic resonances exist at deep-UV wavelengths, so few reports are focused on nano-apertured UV metasurfaces. Moreover, it is still an open question whether the nano-apertures can be used to manipulate the phase of deep-UV light due to the absence of plasmonics.

Here, we investigate both the amplitude and phase modulation of UV light by using nano-apertured metasurfaces without plasmonic resonances. To mimic it, these nano-apertures are experimentally fabricated in a gold film, which excludes

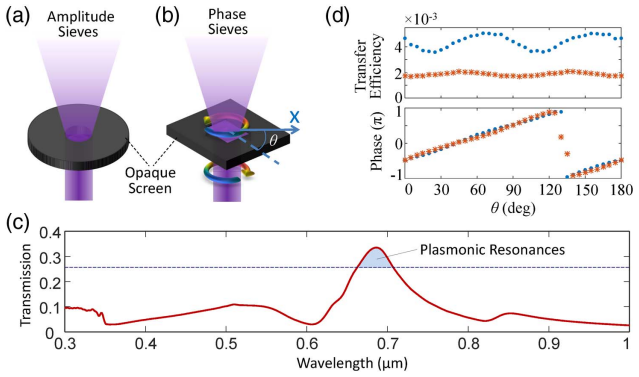

Fig. 1. (a) Sketch of a circular nanosieve for manipulating the amplitude of light. (b) Sketch of a helical nanosieve for phase modulation of circularly polarized light through the orientation angle of θ. (c) Optical transmission of the nanohole array in a 100-nm-thick gold film over the spectrum from 300–1000 nm. The diameter of the hole is 200 nm and the period of the array is 350 nm, which indicates maximum transmission of 25.65% (dashed line) based on its geometry. As denoted by the shadow region, the surface plasmonic resonances happen when the calculated transmission is larger than 25.65%. (d) Simulated transfer efficiency (upper) and phase (lower) of helical nanoiseve with its rotating angle θ varying (from 0–180 with a step of 5). The perfect electric conductor (PEC, dots) and gold (orange asterisks) are used as the materials of the film, as a comparison.

the plasmonic responses at the operating wavelength of 355 nm. Circular and rotated rectangular apertures are proposed to tailor the amplitude and phase of UV light, respectively. A binary-amplitude hologram made of a circular nano-aperture array is designed and fabricated to reconstruct three isolated images at the different cut planes. A phase-type hologram composed of rotating rectangular nano-apertures is also demonstrated to show a holographic image with a modulating range of 2π, which implies the feasibility of phase modulation in the deep-UV range when the plasmonic resonances are absent.

Figures 1(a) and 1(b) sketch the mechanisms of amplitude- and phase-modulation apertures made in an opaque film. In our case, the gold film is used here to avoid the excitation of surface plasmons at a wavelength of 355 nm, as illustrated in Fig. 1(c). It allows us to investigate the control of light by using only the geometry of apertures. Thus, its underlying physics is the same as that of shaping light in the deep-UV spectra, so that the results achieved in this Letter could be extended to the EUV and soft x-ray spectra. In Fig. 1(a), the amplitude modulation is implemented by using a photon nanosieve that contains randomly distributed circular nanoholes with the same diameters [15]. It works as a binary-amplitude mask where the nanohole part has the normalized amplitude of 1 and the left part is blocked with the transmission of 0. The transmission of light passing through the hole is determined by the diameter of the holes, thickness and materials of the film, and materials within the hole [20]. The holes with larger diameters in a thinner film lead to higher transmission. If the material of the film is chosen properly at the working wavelengths, the plasmonics will be induced so that the transmission might be enhanced. In addition, if the holes are filled with materials with a high refractive index of n, the efficient wavelength in the hole is scaled down by $1/n$, which could also increase the transmission of light. Since we focus on the feasibility of manipulating light in the deep-UV spectrum where both the plasmonics and transparent materials are absent, the material issues for efficiency enhancement are not taken into account here.

The proposed phase modulation is realized by using the rotating nano-apertures with a rectangular shape, as shown in Fig. 1(b). In this configuration, a circularly polarized (CP) light passes through the rectangular nano-apertures and is transferred partially into the cross-polarized transmitted light with an additional phase of $e^{i2\theta}$, where θ denotes the angle between the x axis and the long axis of rectangular apertures [16,21]. The achieved phase originates from the coupling between the CP light and the rotation of coordinates, which yields the so-called geometric or Berry phase [22]. The conversion efficiency from the incident polarization to its crossed polarization depends on the electromagnetic interaction in terms of electric and magnetic dipoles [23] or the induced plasmonics [9]. Therefore, it is important to investigate conversion efficiency when electromagnetic interaction is weak or absent. To mimic it, we still use the gold film with strong absorption at a wavelength of 355 nm, thereby excluding the plasmonics. The rectangular aperture with a length of 230 nm and width of 110 nm in a 170-nm-thickness film is exemplified to investigate conversion efficiency. In our simulations implemented by using the finite-difference time-domain method in a pixel pitch of 350 nm $*$ 350 nm, the perfect electric conductor (PEC) and gold (Palik [24]) are used as materials for the film for a comparison. In Fig. 1(d), the simulated efficiency has a value of 0.2%–0.4% over the different rotations of nano-apertures. The results for the PEC and gold films yield efficiency at the same level, which indicates that the gold film is a good approximation of PEC at UV wavelengths. Moreover, the simulated phase modulation of cross-polarized light is twice that of the rotating angle, as predicted by the analytical model.

To verify the feasibility of our proposed methods, we experimentally demonstrate amplitude- and phase-type holograms by using circular and rectangular nano-apertures, respectively. The binary-amplitude nanosieve holograms have been demonstrated with only one holographic image at visible and infrared wavelengths [14]. To exploit its capability further, we investigate three-dimensional nanosieve holograms that could generate some different images during propagation. Figure 2(a) shows that light through the location-optimized holes interferes constructively at the longitudinal positions, which holds the underlying physics of this three-dimensional nanosieve hologram. When the hole has a diameter smaller than one wavelength, the vector effect of its diffracted field must be considered if one needs the high-accuracy manipulation of light [15]. In some cases, if the hole size is much smaller than the propagating distance between the nanosieves and the longitudinal plane of interest, the illuminated hole can be taken as an ideal point source whose radiating field could be approximated by using the discrete Rayleigh–Sommerfeld diffraction [14]. Here, the employed holes have the same diameters of 200 nm, and the distances between the nanosieves and three targeted planes are 200 μm, 300 μm, and 400 μm. It implies that the diffracted field of light passing through the nanosieve hologram could be calculated as a summation of multiple point sources by addressing the locations of the holes. The optimization of holes is carried out by using modified genetic

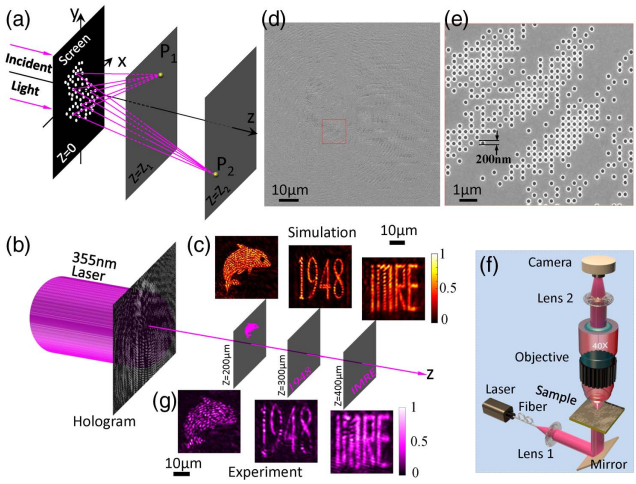

Fig. 2. Demonstration of a three-dimensional nanosieve hologram. (a) Principle for a three-dimensional hologram with constructive interference at different z-cut planes. (b) Sketch for a nanosieve hologram generating three images at different planes. (c) Simulated holographic images. (d), (e) SEM images of the fabricated mask with different fields of view. The SEM image in (e) is a zoomed image encircled in the red rectangle in (d). (f) Experimental setups for measuring holographic images. (g) Measured images by using CCD.

algorithms [15], where the cost function is minimized by decreasing the difference between the ideal and simulated images at three z-cut planes. Our optimized nanosieve hologram with the size of 90 μm ∗ 90 μm is shown in Fig. 2(b), where the simulated images of a dolphin pattern, "1948," and "IMRE" at $z = 200$ μm, 300 μm, and 400 μm are also provided in Fig. 2(c). The hologram is fabricated in a 170-nm-thick gold film (e-beam evaporated on a quartz substrate) by using focused-ion-beam (FIB) lithography with a milling current of 93 pA and a dwell time of ∼10 min. The scanning-electron-microscope (SEM) images of our fabricated hologram are shown with different fields of view in Figs. 2(d) and 2(e), indicating a good profile.

To experimentally characterize the nanosieve hologram, a self-made measurement system is built in a confocal microscopy as sketched in Fig. 2(f). A 355-nm-wavelength laser of ∼10 mw is coupled into a single-mode fiber and used to illuminate the hologram after being collimated by using a lens. The transmitted light through the hologram is collected by using an objective lens (40×) and then projected onto a charge-coupled-device (CCD) camera by a tube lens. The objective lens, tube lens, and CCD are mounted onto a high-precision z-travel stage, thus allowing us to map three images at different planes. The recorded holographic images as shown in the bottom panel in Fig. 2(g) have good agreement with the simulated ones. The slight deviation in details in the images might be caused by the imperfect alignment of optical components, which can be improved by using a higher-power laser for better sight during tuning the optical path. These experimental results confirm that the nanosieve hologram has the ability to generate three-dimensional images and is still valid for the case of weak electromagnetic resonances.

A rectangular nano-aperture array is proposed to demonstrate the metasurface hologram with geometric phase.

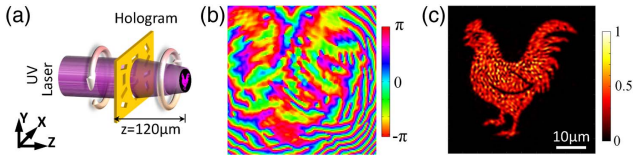

Fig. 3. (a) Sketch for generating a geometric hologram by using helical nanosieves to manipulate phase of spin light. (b) Designed phase profile with a total size of 42 μm × 42 μm. (c) Simulated holographic image with a "cock" pattern.

Figure 3(a) sketches the working principle of this meatsurface hologram. A left-handed CP light is used to illuminate this rectangular nano-aperture array that can partially change the incident light into a right-handed CP light with the designed phase, thus generating the holographic image at the target plane of $z = 120$ μm. A Gerchberg–Saxton algorithm [23] with 100 iterations is used to design the required phase with a size of 42 μm × 42 μm, as shown in Fig. 3(b). Correspondingly, the simulated holographic image has a pattern of "cock" in Fig. 3(c). For a highly coherent laser, the holographic image has unavoidable speckles that, however, can be efficiently suppressed by increasing the size of the hologram [4]. To realize the designed phase, we experimentally fabricate the nano-aperture array by using FIB lithography with a milling current of 93 pA and dwell time of ∼20 min. Figure 4(a) shows the SEM image of our fabricated sample where the phase is discretized into 16 levels. For example, the phase φ_n is realized by a rectangular aperture with its orientation angle of $\varphi_n/2$. The rectangular shape with high uniformity can be observed in the entire sample, indicating good fabrication. Its experimental measurement is implemented in the same confocal microscopy by adding two pairs of linear polarizers (LPs) and quarter-wave plates (QWPs), which are, respectively, used as the CP polarizer (LP1 and QWP1) and analyzer (LP2 and QWP2) in Fig. 4(b). The experimentally captured image is shown in Fig. 4(c), which shows the expected pattern of "cock."

Although the efficiency is much lower than those at visible and infrared wavelengths, it is of important significance to introduce customized phase modulation when the electromagnetic

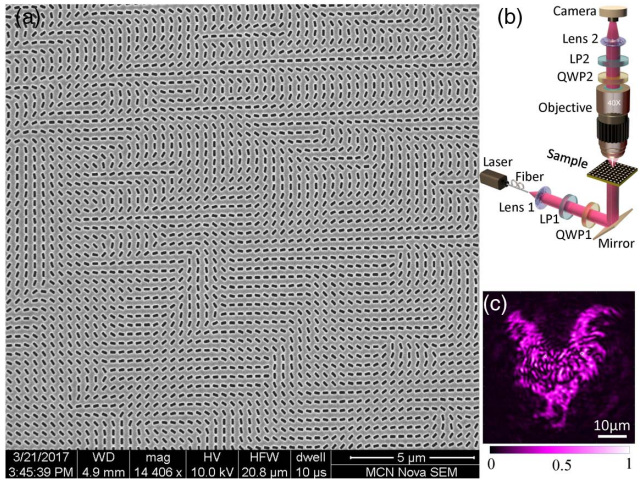

Fig. 4. (a) SEM image of the fabricated sample. (b) Experimental setup for measuring the hologram. (c) Measured holographic image.

responses are weak. Such a phase induced by the geometry of structures provides more degrees of freedom in wavefront shaping at the EUV and x-ray wavelengths than the accumulated phase by the density of gases [25]. In our proposal, the pixel pitch of 350 nm is subwavelength compared with the working wavelength of 355 nm. Thus, this mechanism could be extended to the EUV spectrum (5 nm $< \lambda <$ 100 nm) because it is feasible to fabricate the structures with a feature size of tens of nanometers by using state-of-the-art nanolithography. Due to low efficiency, the EUV devices in this mechanism should work in an off-axis way, so that the signal light with the modulated phase can be separated from the un-modulated background. For this nano-aperture array with geometric phase, conversion efficiency could be enhanced by decreasing the pixel pitch of the array, which increases the density of apertures in a fixed area.

In summary, we have demonstrated the amplitude and phase modulation of UV light by using a nano-aperture platform when electromagnetic interaction is weak or absent. The demonstrated binary-amplitude and multi-level phase holograms with subwavelength pixel pitches behave well for optical holographic imaging in the UV spectrum. Due to the absence of plasmonics, this proposed mechanism could be extended to the manipulation of EUV light, which might benefit across UV photonics and nano-lithography.

Funding. CAS Pioneer Hundred Talents Program; National Natural Science Foundation of China (NSFC) (61705085, 61875181); "The Fundamental Research Funds for the Central Universities" in China.

Acknowledgment. This work was partially carried out at the University of Science and Technology of China's Centre for Micro and Nanoscale Research and Fabrication.

†These authors contributed equally to this Letter.

REFERENCES

1. D. Attwood and A. Sakdinawat, *X-Rays and Extreme Ultraviolet Radiation: Principles and Applications* (Cambridge University, 2017).
2. J. D. Koralek, J. F. Douglas, N. C. Plumb, Z. Sun, A. V. Fedorov, M. M. Murnane, H. C. Kapteyn, S. T. Cundiff, Y. Aiura, K. Oka, H. Eisaki, and D. S. Dessau, Phys. Rev. Lett. **96**, 017005 (2006).
3. T.-J. Lu, M. Fanto, H. Choi, P. Thomas, J. Steidle, S. Mouradian, W. Kong, D. Zhu, H. Moon, K. Berggren, J. Kim, M. Soltani, S. Preble, and D. Englund, Opt. Express **26**, 11147 (2018).
4. K. Huang, J. Deng, H. S. Leong, S. L. K. Yap, R. B. Yang, J. Teng, and H. Liu, Laser Photon. Rev. **13**, 1800289 (2019).
5. N. Yu, P. Genevet, M. A. Kats, F. Aieta, J.-P. Tetienne, F. Capasso, and Z. Gaburro, Science **334**, 333 (2011).
6. P. Lalanne, S. Astilean, P. Chavel, E. Cambril, and H. Launois, Opt. Lett. **23**, 1081 (1998).
7. Z. Bomzon, V. Kleiner, and F. Hasman, Opt. Lett. **26**, 33 (2001).
8. L. Zhang, S. Mei, K. Huang, and C.-W. Qiu, Adv. Opt. Mater. **4**, 818 (2016).
9. G. Zheng, H. Mühlenbernd, M. Kenney, G. Li, T. Zentgraf, and S. Zhang, Nat. Nanotechnol. **10**, 308 (2015).
10. M. Semmlinger, M. L. Tseng, J. Yang, M. Zhang, C. Zhang, W.-Y. Tsai, D. P. Tsai, P. Nordlander, and N. J. Halas, Nano Lett. **18**, 5738 (2018).
11. Y. Deng, X. Wang, Z. Gong, K. Dong, S. Lou, N. Pégard, K. B. Tom, F. Yang, Z. You, L. Waller, and J. Yao, Adv. Mater. **30**, 1802632 (2018).
12. C. Argyropoulos, F. Monticone, G. D'Aguanno, and A. Alù, Appl. Phys. Lett. **103**, 143113 (2013).
13. A. M. Watson, X. Zhang, R. Alcaraz de La Osa, J. M. Sanz, F. González, F. Moreno, G. Finkelstein, J. Liu, and H. O. Everitt, Nano Lett. **15**, 1095 (2015).
14. K. Huang, H. Liu, G. Si, Q. Wang, J. Lin, and J. Teng, Laser Photon. Rev. **11**, 1700025 (2017).
15. K. Huang, H. Liu, F. J. Garcia-Vidal, M. Hong, B. Luk'yanchuk, J. Teng, and C.-W. Qiu, Nat. Commun. **6**, 7059 (2015).
16. X. Li, L. Chen, Y. Li, X. Zhang, M. Pu, Z. Zhao, X. Ma, Y. Wang, M. Hong, and X. Luo, Sci. Adv. **2**, e1601102 (2016).
17. R. Liu, F. Li, M. J. Padgett, and D. B. Phillips, Optica **2**, 1028 (2015).
18. Y. J. Liu, H. Liu, E. S. P. Leong, C. C. Chum, and J. H. Teng, Adv. Opt. Mater. **2**, 487 (2014).
19. J. Park, K. Lee, and Y. Park, Nat. Commun. **10**, 1304 (2019).
20. F. J. Garcia-Vidal, L. Martin-Moreno, T. W. Ebbesen, and L. Kuipers, Rev. Mod. Phys. **82**, 729 (2010).
21. M. Mehmood, S. Mei, S. Hussain, K. Huang, S. Siew, L. Zhang, T. Zhang, X. Ling, H. Liu, and J. Teng, Adv. Mater. **28**, 2533 (2016).
22. X. Ling, X. Zhou, K. Huang, Y. Liu, C.-W. Qiu, H. Luo, and S. Wen, Rep. Prog. Phys. **80**, 066401 (2017).
23. K. Huang, Z. Dong, S. Mei, L. Zhang, Y. Liu, H. Liu, H. Zhu, J. Teng, B. Luk'yanchuk, J. K. Yang, and C. Qiu, Laser Photon. Rev. **10**, 500 (2016).
24. E. D. Palik, *Handbook of Optical Constants of Solids* (Academic, 1998).
25. L. Drescher, O. Kornilov, T. Witting, G. Reitsma, N. Monserud, A. Rouzée, J. Mikosch, M. J. J. Vrakking, and B. Schütte, Nature **564**, 91 (2018).

222.195.90.168 {ts '2019-07-03 02:43:03'}